Geological Quarterly, 2019, **63** (4): 861–874
DOI: http://dx.doi.org/10.7306/gq.1507

Timing of ore mineralization using ore mineralogy and U-Pb dating, Iron Oxide Copper Gold Sin Quyen deposit, North Vietnam

Jadwiga PIECZONKA[1], Chau Dinh NGUYEN[1], Adam PIESTRZYŃSKI[1, *] and Phon Khanh LE[2]

[1] AGH University of Science and Technology, Faculty of Geology, Geophysics and Environmental Protection, Al. A. Mickiwicza 30, 30-059 Kraków, Poland

[2] Hanoi University of Mining and Geology, Oil and Gas Faculty, Dong Ngac, Tu Liem, Hanoi, Vietnam

Pieczonka, J., Nguyen, C.D., Piestrzyński, A., Le, P.K., 2019. Timing of ore mineralization using ore mineralogy and U-Pb dating, Iron Oxide Copper Gold Sin Quyen deposit, North Vietnam. Geological Quarterly, **63** (4): 861–824, doi: 10.7306/gq.1507

Associate Editor: Jacek Szczepański

Magnetite, pyrite, pyrrhotite, chalcopyrite and sphalerite are the major minerals identified in the deposit, while ilmenite, marcasite, tennantite, cubanite, arsenopyrite, galena, allanite, chevkinite, apatite, Bi-native, bismuthinite, electrum, native gold, and tellurides are the minor ones in the Iron Oxide Copper Gold (IOCG) Sin Quyen deposit. The REEs are hosted mostly by allanite, and the minor minerals by chevkinite, monazite, apatite and uraninite. Based on chemical analyses and Raman spectroscopy, two varieties of allanite have been documented: (1) with lower total REE contents of 13–19 wt.%, and (2) with higher contents of 20–23 wt.%. Uraninite from copper-iron massive ores is inhomogeneous in both optical properties and chemical composition. The concentrations of uranium and total rare earth element oxides (REOs) in the paragenetically earlier uraninite are 84.55–85.96% and 1.9–8.0% on average, respectively, whereas in paragenetically later uraninite, the U and ΣREE_2O_3 concentrations are 96.2–96.7% and 1.3–2.7% on average respectively. The thorium concentration in both the early and late uraninites is very low (0.21–0.22% and 0.2 % on average). These are the highest REE concentrations as compared with the known concentrations of these elements in uraninite. Electron microprobe "chemical" dating of the uraninite yielded an age of 500 ±33 Ma (n = 35) for the paragenetically early uraninite, and an age of 73 ±15 Ma (n = 6) for the paragenetically later ones. The minerals of the older age, which is interpreted as the primary ore mineralization stage, correspond in age with a range of deposits along the East Gondwana margin. The measured $\delta^{34}S$ of sulphide minerals from –2.78 to +8.65‰ suggests hydrothermal origin of fluid that was responsible for transportation and crystallization.

Key words: IOCG deposit, uraninite dating, mineral stages, geochemistry.

INTRODUCTION

The Sin Quyen deposit is the largest IOCG deposit in Vietnam (Pham et al., 2011; Zhao and Zhou, 2011). The following reserves were calculated during the exploration stage: 550,000 t of Cu, 334,000 t REE, 843,000 t S, 34.7 t Ag, and 25.3 t Au (ESCAP, 1990). Since 2006, this deposit has been exploited as an open-pit mine. Each year, six million cubic metres of host rocks and one million tonnes of ore are excavated, and the annual average production of the metallic copper is 12,000 tonnes (Le et al., 2015). In the deposit, the copper concentrations range from 0.55 to 1.93%, and the iron content is ranging from a few to some tens of percents. The total concentrations of rare earth elements range from 12 ppm to more than 5.400 ppm; however, 0.7% of REE was used for reserve calculation (ESCAP, 1990). The REE are not recovered from the deposit. The maximum concentration of the sum of the REE measured in the waste sample was 0.54%.

The IOCG deposits are well-known around the world (Hitzman, 2000; Corriveau et al., 2007), but the studied deposit is a specific variety in which both copper with gold and magnetite rich ore are of economic importance. Due to evidence of formations of both magmatism and metamorphism originating in the deposit region, the origin of this deposit is still discussed (Ta, 1975; McLean, 2001; Tran, 2007; Ishihara et al., 2011; Pham et al., 2011; Pieczonka et al., 2015; Li and Zhou, 2018a, b; Li et al., 2018).

The paper presents the results of determination of the absolute age of uraninite by the U-Pb method CHIME (The Chemical Th-U-Pb Isochrone Method) and investigation of Cu, Fe, Ag, Au, U and REE minerals of some samples collected in site.

* Corresponding author, e-mail: piestrz@agh.edu.pl

Received: January 22, 2019; accepted: October 11, 2019; first published online: December 30, 2019

OUTLINE OF REGIONAL GEOLOGY

Geologically, the territory of North Vietnam is divided by the Red River (Song Hong, and Song Chay) fault system into the Indochina Block in the west and the South China Block in the east (Fig. 1). North-east Vietnam is composed mainly of Devonian terrigenous carbonate suits including shale, black argillite, clayish limestone and marble (Pham et al., 2011), which are a part of the South China Block (Fig. 1). North-west Vietnam is built of Paleoproterozoic to Neoproterozoic terrigenous sediments interbedded with minor carbonate and volcanic rocks forming the Indochina Block (Fig. 1; Phan, 2015). In North Vietnam the Phan Si Pan and Day Nui Con Voi belts constitute parts of the Red River shear zone (Tapponnier et al., 1990; Leloup et al., 2007). The Pan Si Pan belt is a high-grade metamorphic complex including the Suoi Chieng, Sin Quyen and Cam Duong formations. The Suoi Chieng formation is composed of Paleoprotezoic biotite schist, amphibolite and terrigenous sediments. The formation is conformably covered by the Sin Quyen formation with Paleoproterozoic to Neoproterozoic terrigenous sediments interbedded with minor carbonate and volcanic formations. According to the mineral composition, the Sin Quyen formation is divided into upper and lower units. In the upper unit (Sq1), quartz (50%), graphite (15%), muscovite (12%) and biotite (10%) are the major minerals, while plagioclase, tourmaline, garnet are sillimanite are minor ones. The lower unit (Sq2) consists chiefly of plagioclase (61%), quartz (21%) and biotite (15%) as major minerals, and apatite, sphene, calcite and garnet as accessory minerals (Ta, 1975; McLean, 2001). The Cam Duong formation is composed of Paleozoic suits containing quartz, sericite, graphite, carbonate and biotite. The formation extends in the NW–SE direction from 280 to 320° and dips at 20 to 70° (Ta, 1975). In the north-west, the Pan Si Pan belt complex is intruded by Neoprotezoic and Upper Permian and Lower Triassic igneous rocks. The Day Nui Con Voi belt is composed of limestone, mafic olistoliths and mudstone matrix with slumped beds suggesting gravity-driven chaotic sedimentation (Faure et al., 2014). The Sin Quyen copper deposit, nearly 2 km^2 in area, is located 300 km NW of Hanoi, close to the China border. This deposit is composed of 17 ore bodies with an average grade of 0.91 wt.% Cu, 0.7 wt.% LREE (La, Ce, Pr and Nd) and 0.44 ppm Au; the total expected Cu resource is 550,000 tons (Ta, 1975; McLean, 2001). The ore bodies occur as lens, up to tens of metres thick and a few hundred metres long, trending NW–SE and dipping nearly vertically (70–80°) (Fig. 2). The Copper Sin Quyen deposit has been exploited since 2006 (Phan, 2015). The main ore minerals are magnetite, pyrite, pyrrhotite, chalcopyrite, allanite and some minor minerals: ilmenite, marcasite, sphalerite, tennantite, cubanite, arsenopyrite, galena, native bismuth, bismuthinite, electrum, native gold, and tellurobismuthite.

METHODS

Forty-four samples were collected from the deposit, three from waste and two from copper and iron concentrate; the sampling places are shown in Figure 3. All samples were studied in detail using an optical microscope both in transmitted and reflected light. Based on this investigation, some samples were

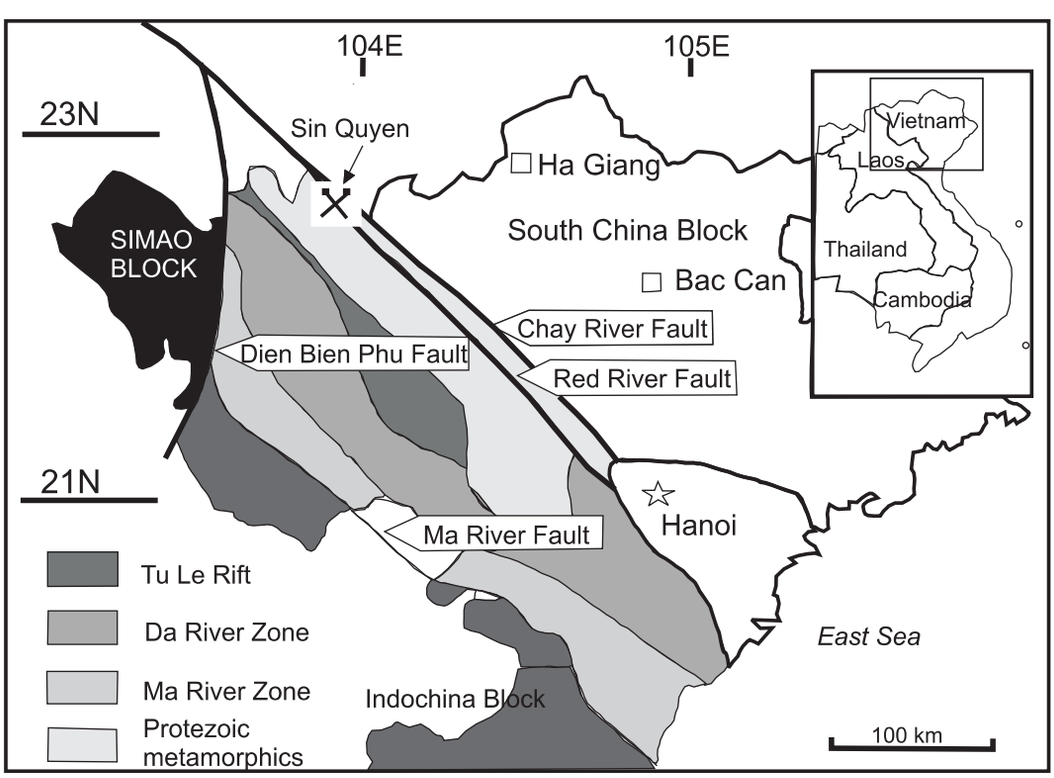

Fig. 1. Geological sketch-map of North Vietnam with the location of the Sin Quyen deposit (after McLean, 2001, modified)

Fig. 2. The view of the main magnetite ore body in the Sin Quyen deposit (phot. 2015, looking NW)

selected for the bulk chemical analyses and EDS and WDS measurements (Table 1).

The bulk chemical analyses of the waste, concentrates and solid samples were carried out at ACME Laboratories in Vancouver Canada, using the AQ251 method. The sample of 0.5 g was digested in aqua regia at 90°C, followed by an ICP-MS procedure. Analytical uncertainties are 5% of the measured value for most analysed elements. Detection limits for REE vary from 0.02 to 0.5 ppm, and for U and Th are equal to 0.1 ppm, and are standard for the AQ251-type analyses (ACME, www.acmelab.com).

Electron microprobe measurements were carried out in the Critical Element Laboratory of the AGH-UST University in Kraków. The following standards and measurement lines have been used: SiKα (albite), AlKα (kyanite), SKα (anhydrite), UMβ (UO_2), YLα (YPO_4), PKα (YPO_4), ScKα (100%), TiKα (rutile), CeLα ($CePO_4$), LaLα ($LaPO_4$), ThMα (ThO_2), CaKα (wollastonite), PrLβ (PrPO4), TbLα ($TbPO_4$), DyLα ($DyPO_4$), ErLα ($DyPO_4$), LuLα ($LuPO_4$), GdLβ ($GdPO_4$), PbMα (crocoite), NdLα ($NdPO_4$), SmLα ($SmPO_4$), EuLβ ($EuPO_4$), TmLα ($TmPO_4$), YbLα ($YbPO_4$), HoLβ ($HoPO_4$), AsLα (InAs). Overlap correction of Nd-Ce, Sm-Ce, Lu-Dy, Dy-Eu, U-Th, Tm-Sm and Gd-Ho were implemented using the method described by Pyle et al. (2002).

The following conditions were implemented for WDS measurements: accelerating voltage 15 kV, probe current 40 nA, focused electron beam diameter 3 μm; counting times peak/background (in sec.) were as follows: Si 10/5, Al 10/5, S 20/10, REE 45/15, P 20/10, Ti 20/10, Ca 20/10, V 10/5, Fe 20/10 and As 20/10. For better statistics of measurements and to reduce the detection limit, the following peak/background conditions (in sec.) were used: U 120/60, Pb 180/90, Th 120/60. Original Jeol ZAF procedures were used for the final correction of all measured elements. Monazite crystal TS-Mnz (894.8 ±5.3 Ma) was used as a reference material for microprobe standardization (Budzyń et al., 2017).

The analyses of $\delta^{34}S$ in seven mineral separates of chalcopyrite, pyrrhotite and mixed chalcopyrite-pyrrhotite were undertaken at Maria Curie-Skłodowska University (UMCS) in Lublin, Poland. Prior to $\delta^{34}S$ analysis, ~0.5 g of separate was separated from the massive sulphide ore, dried at 90°C, powdered to the 100–200 μm and homogenized. A small aliquot of this mineral separate was analysed using an element analyser attached to an *Isotope Relative Mass Spectrometer* (IRMS) (Pearson Jr. and Rightmire, 1980), with results reported relative to Vienna Canyon Diablo Troilite (V-CDT). The 1δ precision is ±0.2‰.

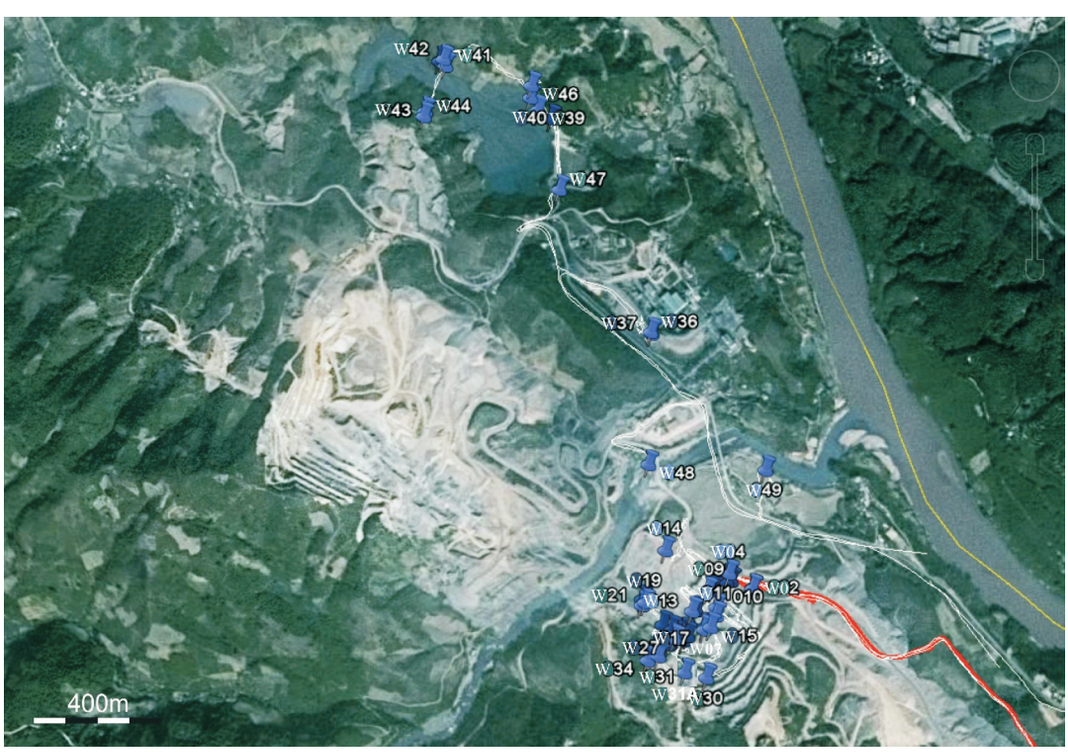

Fig. 3. Location of collected samples on the Google map

Table 1

The list of samples used for detailed investigations

Sample	Location	Type of rocks	Remarks
W-3	open pit	Fe-Cu ore with allanite	mineralogy, WDS, Raman spectroscopy
W-5	open pit	magnetite-copper ore	mineralogy, WDS, age determination
W-7	open pit	massive copper ore	chalcopyrite, $\delta^{34}S$
W-15	open pit	dispersed – laminated Cu ore	mineralogy, bulk chem. analysis
W-18	open pit	massive Cu ore, chalcopyrite	mineralogy, bulk chem. analysis
W-25	open pit	epidote- amphibolite rock	mineralogy, bulk chem. analysis
W-31	open pit	skarn	mineralogy, bulk chem. analysis
W-31a	open pit	garnet skarn	mineralogy, bulk chem. analysis
W-33	open pit	disseminated/massive ore	chalcopyrite, pyrrhotite, $\delta^{34}S$
W-36	floatation plant	copper concentrate	mineralogy, bulk chem. analysis
W-37	local storage	iron concentrate	mineralogy, bulk chem. analysis
W-39	lower tailing	waste I	mineralogy, bulk chem. analysis
W-40	lower tailing	waste II	mineralogy, bulk chem. analysis
W-44	pipeline transporting waste	waste outflowing from the pipe	mineralogy, bulk chem. analysis

Location of samples is shown in Figure 3

RESULTS AND DISCUSSION

GEOCHEMISTRY OF HOST ROCKS, ORE, CONCENTRATES AND WASTES

Based on microscopy of ore samples, magnetite, pyrite, pyrrhotite, chalcopyrite, sphalerite are major minerals and ilmenite, marcasite, tennantite, cubanite, arsenopyrite, galena, Bi-native, bismuthinite, electrum, native gold, and tellurides are minor ones. All the above-mentioned minerals are characteristic for ores occurring in the skarn zone. The copper content ranges from tens of ppm to the level above 1.0 wt.%, with an average of 0.3 wt.%; the iron content reaches 40 wt.%. The precious metals are highly variable, the gold concentrations in ore samples range from 3 to 2.360 ppb with an average of 482 ppb, and the silver concentrations range from 8 to 1.850 ppb with an average of 422 ppb (Appendix 1A*). The average values of these metals are a few hundred times larger than those in the Earth's crust. The extra-high concentrations of Au (6.500 ppb), Ag (31.000 ppb), Zn, Co, Se and Te are observed in the copper concentrate (Appendix 1A). High Ag and Au contents are commonly associated with the high copper content, suggesting an association with chalcopyrite. In some Au-Ag-rich samples (e.g., W-36), elevated concentrations of uranium and thorium are also reported, as also noted by McLean (2001) and Gaskov et al. (2012). Sample W-25 shows a relatively high concentration of niobium (227 ppm), sample W-18 and the Fe-concentrate (sample W-37) have enrichments in vanadium (123 and 219 ppm, respectively).

The samples are characterized by low concentrations of Ti (Appendix 1A), which is typical for the IOCG deposits (Dupuis and Beaudoin, 2011; Fengli et al., 2014; Chen et al., 2015). The maximum concentrations of REE, up to 5.470 ppm, were found in tailing samples (W-39, W-40, and W-44; Appendix 1B). The REE occur mostly in minerals of the allanite group (Pieczonka et al., 2017). In some polished sections prepared from the ore, the concentration of allanite reaches 1 to 5% by volume (e.g., sample No. 3). The highest uranium concentrations (56 ppm) were found in sample W-18 collected at the site displaying the highest intensity of gamma-ray radiation in the ore bodies, which is typical of massive Cu-Fe ore (Nguyen et al., 2016). The elevated amounts of U and Th are noted also in the waste samples (W-39, W-40 and W-44; Appendix 1A) and are related to the uraninite and allanite groups.

ORE MINERALS DESCRIPTION

Several types of ore are recognized in the deposit:
- massive copper ore,
- massive iron ore,
- mixed Fe-Cu ore,
- dispersed ores,
- vein-type ore and supergene weathered ore (Fig. 4).

All ore types are characterized by different ore mineral assemblages. Based on the space distribution of the major minerals within the deposit, Gaskov et al. (2012) divided the deposit into two zones. In the first zone, located in the central and eastern part of the deposit, pyrite, pyrrhotite and chalcopyrite are dominant, while in the second, western zone – chalcopyrite and magnetite are the prevailing ore minerals. Major ore minerals include magnetite, pyrite, pyrrhotite, chalcopyrite and allanite; minor and

* Supplementary data associated with this article can be found, in the online version, at doi: 10.7306/gq.1507

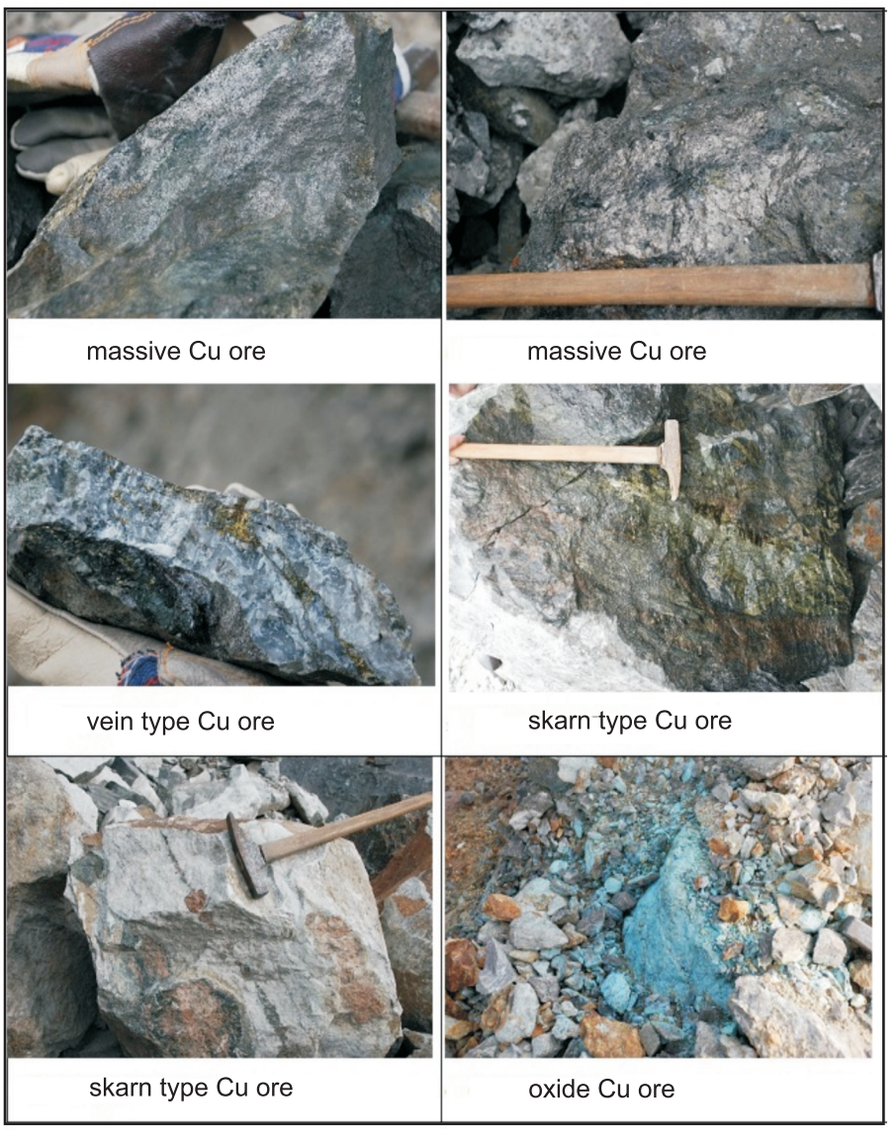

Fig. 4. Different ore types

trace minerals include ilmenite, marcasite, sphalerite, tennantite, cubanite, arsenopyrite, galena, uraninite, native Bi, bismuthinite, electrum, native gold and tellurobismuthite (Figs. 5 and 6). In magnetite-dominant ores, chalcopyrite is very common, while in massive copper ore, magnetite and pyrrhotite are major associated minerals. Electrum was recognized in massive sulphide ores as 1–5 μm thick veinlets and as 5–100 μm inclusions and veinlets randomly distributed in pyrite and chalcopyrite (Figs. 5C and 7). EDS measurements indicate an average composition of 75.72% Au and 24.28% Ag, which confirmed microscopic observation and the presence of electrum. Using the same methods, a Bi-S and Bi-Te mineral association was documented (Fig. 5D). This association is composed of tellurobismuthite, containing 87.62 wt.% of Bi and 21.38 wt.% of Te (EDS composition), and bismuthinite (Fig. 5D).

SULPHUR ISOTOPES

Sulphur isotopes of selected sulphides from massive and disseminated types of ore have been analysed. The value of $\delta^{34}S$ varies from –2.78 to +8.65‰ (Table 2). Similar values of $\delta^{34}S$ are noted in publication by Li and Zhou (2018b) and Li et al. (2018). Such values might suggest post-magmatic hydrothermal origin of sulphur which was transported by fluids responsible for crystallization of the ore mineral assemblage (Thode, 1991). The massive copper ore is composed of chalcopyrite, pyrrhotite, cubanite, magnetite, pyrite and allanite (as major components), arsenopyrite, sphalerite, tennantite and marcasite (as minor minerals), and traces of galena and a Bi-Te-precious metal association. The presence of exolutions of sphalerite stars in chalcopyrite suggests high temperature of sulphide crystallization, but not higher than 500°C (Sugaki et al., 1987). It depends on temperature, pressure and Zn concentration in chalcopyrite (Sugaki et al., 1987). The massive iron ore is composed of magnetite, allanite, pyrrhotite, minor pyrite, chalcopyrite and cubanite, and traces of uraninites. The mixed Fe-Cu ores are represented by both associations mentioned above. Other types of mineralization are minor in the deposit. Except Cu sulphides, more important minerals are represented by allanites and uraninite, which are important carriers of the REE, U and Th.

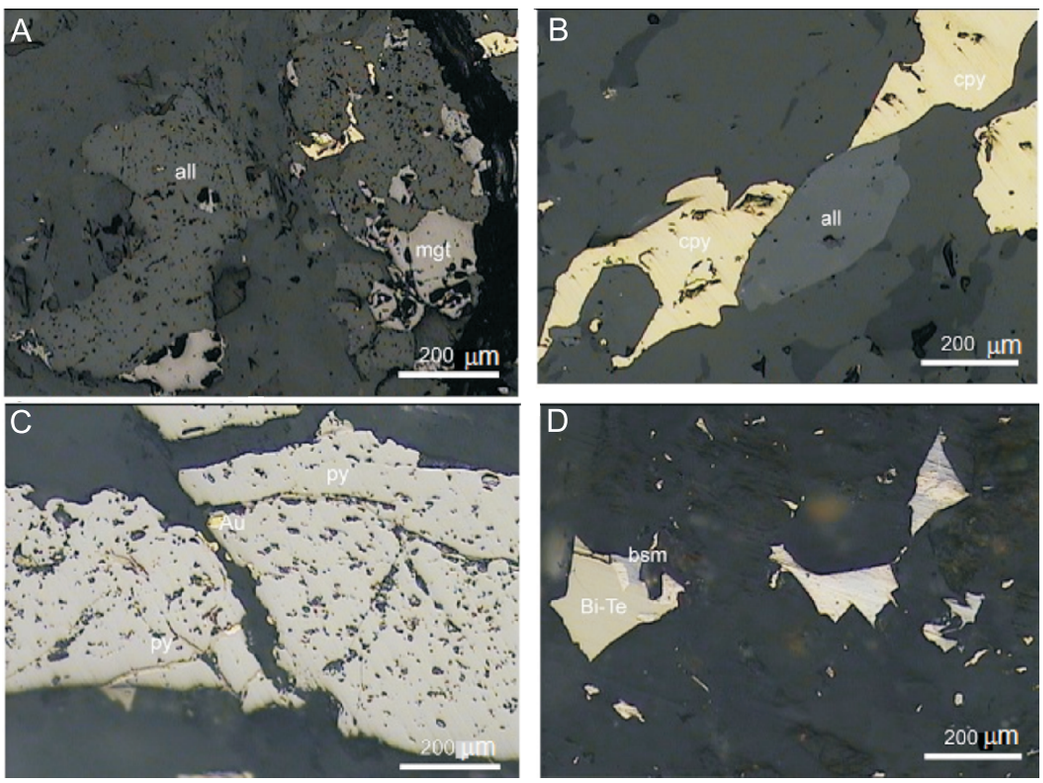

Fig. 5. Microphotographs of principal ore minerals

A – intergrowth of allanite (all) with magnetite (mgt), white – sulphides, reflected light; **B** – intergrowth of allanite (all) with chalcopyrite (cpy), reflected light; **C** – position of gold (Au) with pyrite (py), reflected light; **D** – Bi-Te assemblage (Bi-Te – tellurobismuthite, bsm – bismuthinite), pale yellow – chalcopyrite, reflected light

Table 2

ä34S data of the selected sulphide minerals from the Sin-Quyen deposit (UMCS Lublin Lab.)

Sample	Minerals	Type of ore	$\delta^{34}S‰$
W-18	chalcopyrite	breccia cement	+8.65
W-33	chalcopyrite, pyrrhotite	disseminated ore	+3.06
W-31	chalcopyrite, pyrrhotite	disseminated ore	+2.57
W-15	pyrrhotite	massive ore	+8.27
W-7	pyrrhotite	massive ore	-2.78
W-18	chalcopyrite	massive ore	+0.93
W-33	chalcopyrite (75%), pyrrhotite	massive ore	+2.57

URANINITE

Uraninite was described by McLean (2001), but no special attention was paid to it in that publication. Uraninite was thoroughly described in the project grant No. 01/2012/HD-HTQTSP, because the identification of radioactive materials was one of its major aims. Uraninite crystals have been found in the magnetite sulphide massive ores (Fig. 6). The crystals of uraninites are up to 150 µm in size and are mostly intergrown with magnetite and sulphide minerals. Some euhedral crystals have been found as inclusions in magnetite and silicate minerals matrix, e.g. biotite. These relationships are good indications that uraninite crystallized simultaneously with magnetite within the ore. The uraninites are inhomogeneous especially in high magnification under optical microscope. The inhomogeneity appears in slight colour tint changes, reflectivity and internal reflections. This inhomogeneity was visible in both WDS analysis (Appendix 2) and BSE image (Fig. 8).

The composition of uraninite is variable, particularly with respect to both rare earth element oxides (REEOs) and PbO. The high Pb-bearing uraninite (5.0–6.8 wt.% PbO) tends to have also higher REEOs (1.9–8.0 wt.%), whereas in the low Pb-uraninite (0.54–1.06 wt.% PbO) there is lower total REEOs (1.3–2.7 wt.%). The uraninites with a high concentration of REEOs and high PbO reaching 8 wt.% (Appendix 2) are classified as older. These uraninites can be related to basement fluids (Alexandre et al., 2015). The concentration of Pb in the host rocks and ore is very low (4.32 ppm), while in the waste it is only 4.83 ppm; even in the copper sulphide concentrate it is also low – 40.8 ppm (Appendix 1A). Such low Pb in all deposit materials

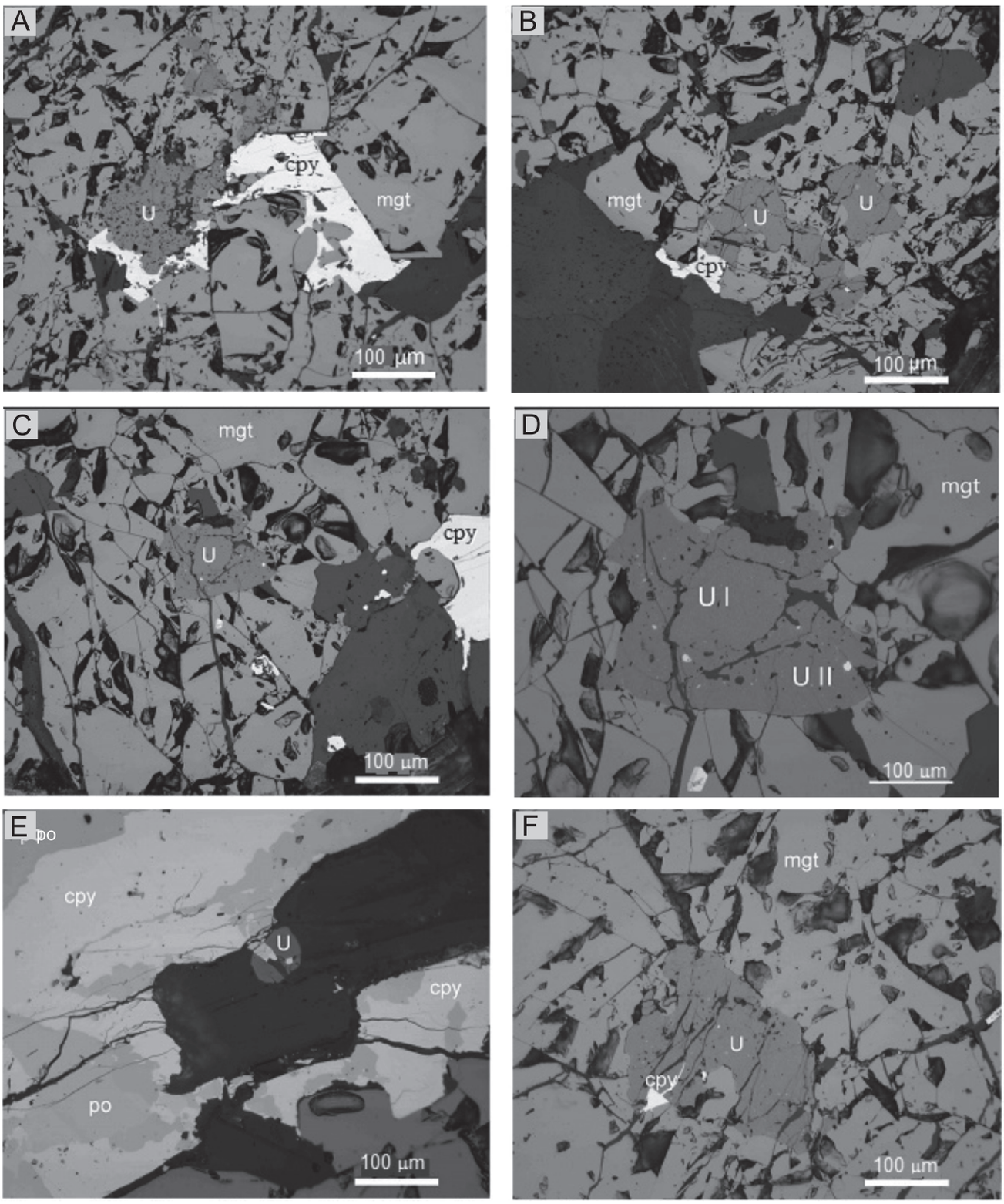

Fig. 6. Microphotographs of uraninite aggregates

A – intergrowth of uraninite (U) with magnetite (mgt) and chalcopyrite (cpy), reflected light; **B** – intergrowth of uraninite (U) with magnetite (mgt) and chalcopyrite (cpy), reflected light; **C** – intergrowth of uraninite (U) I and II with magnetite (mgt) and chalcopyrite (cpy); allanite (all), reflected light; **D** – intergrowth of two different uraninites UI and UII with magnetite (mgt), reflected light; **E** – a small uraninite crystal (U) in silica matrix, po – pyrrhotite, cpy – chalcopyrite, reflected light; **F** – intergrowth of uraninite (U) with magnetite (mgt) and younger chalcopyrite II (cpy), reflected light

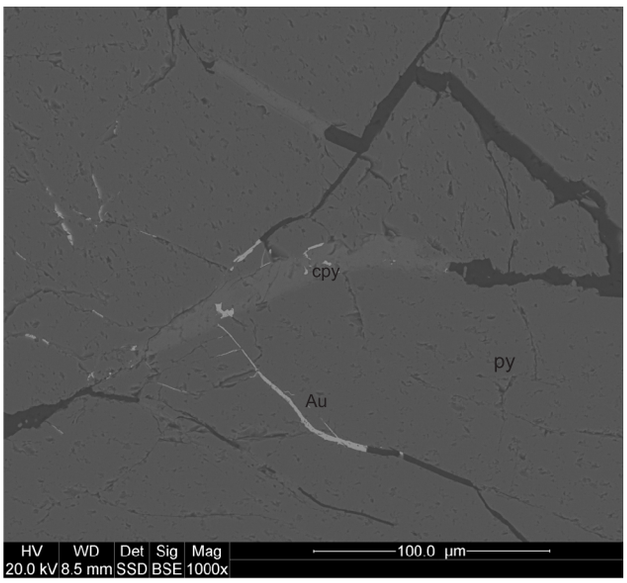

Fig. 7. BSE image showing position of electrum (Au) in relation to pyrite (py) and chalcopyrite (cpy)

indicates the lack of Pb leaching. Therefore, the Pb level relation in the deposit is different from the model described by Janeczek and Ewing (1995), in which thermal regional activity can leach Pb from the uraninites. In the paper, uraninite grains characterized by different contents of REE and textural relationship have been classified into two different stages (Table 3 and Fig. 8). The argumentation can support that the absolute age presented in this work seems to be realistic, and the younger uraninite show only the last hydrothermal event related to tectonic or young volcanism which is documented in the area. Therefore uncertainty of age determination can be larger (Appendix 2, Fig. 9). The low-Pb, and low REE contents in uraninite could be a result of recrystallization of the high-Pb, high-REE uraninite, as shown in BSE images (Fig. 8).

Such minerals as chevkinite, aeschynite, bastnäsite and fluorapatite are rare in the ores, and their influence on the total volume of REE in the deposit is low. The rock-forming minerals contain some REE but below the level of WDS measurements.

Uraninites representing the final alteration stage show variable ages (Appendix 2, Fig. 9). REE concentrations in young uraninite are relatively high compared to that in other examples of natural uraninite described by Alexandre et al. (2015). The

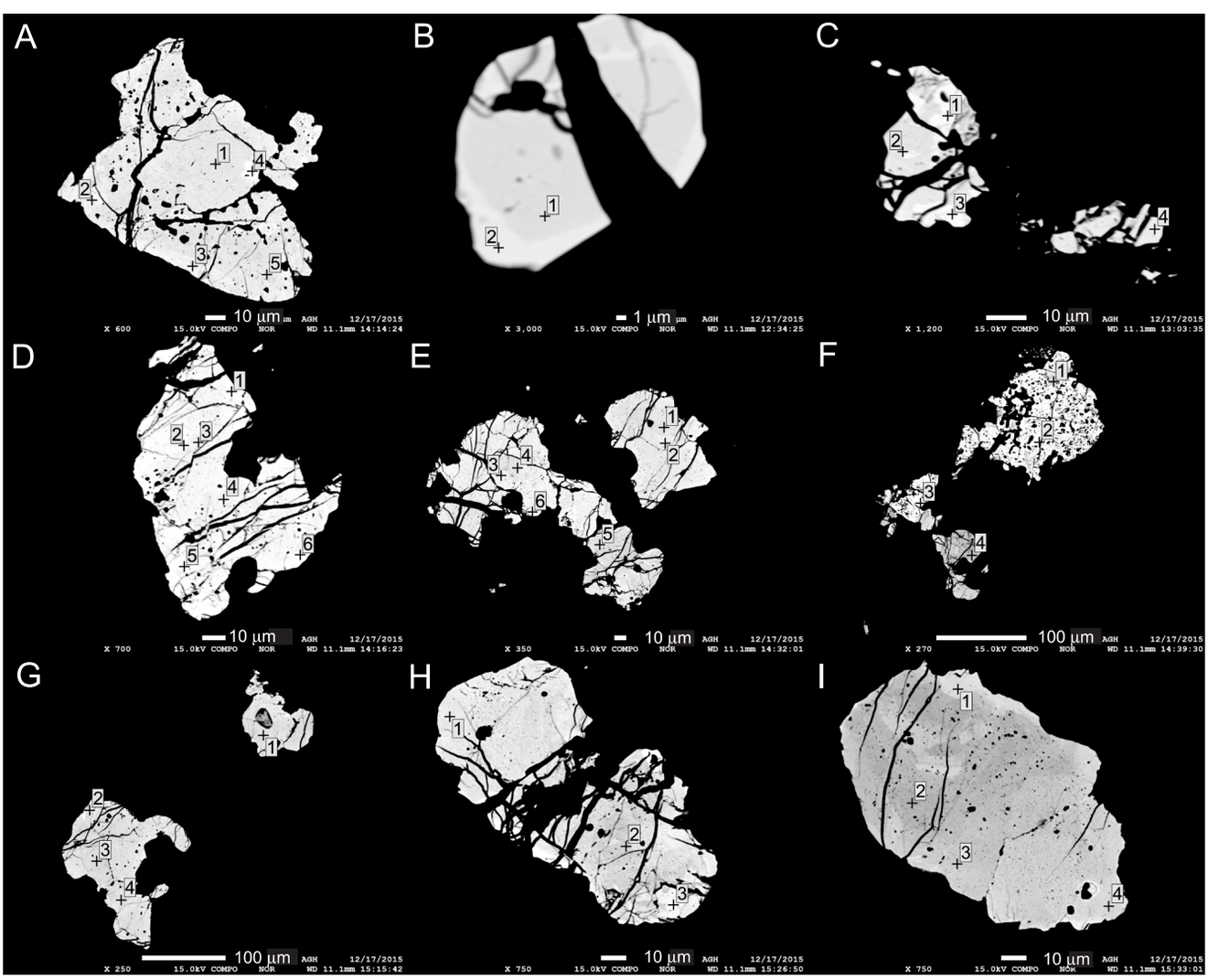

Fig. 8. BSE images showing location of WDS quantitative analyses within the uraninite grains and points of absolute age determinations (+): A–I separate grains of uraninite, samples Nos. 3 and 5

Table 3

Timing of ore mineralization in the Sin Quyen deposit (partly after Ta, 1975; McLean, 2001; Li et al., 2018)

Mineral	Na-alteration stage 841-836 Ma	Skarn-Metasomatic stage 575-430 Ma	Hydrothermal stage 82-42 Ma	Weathering stage
Albite [2)]	----------	--		
Zircon[2)]	—	-		
Monazite[1)]	--?			
Biotite		———————		
Hedenbergite		————		
Hessonite		————		
Hastingsite		————		
Hematite		------		
Quartz I	------ (I)	———— (II)	------- (III)	
Titanite		----		
Epidote		--------		
Rutile		----		
Ilmenite		----		
Allanite	——-	-------	— (II)	
Chlorite		----------		
Calcite		----------	-----	
Basnäsite[1)]		-?		
Apatite		--		
Magnetite	--?	-----———————		
Uraninite		-----(I)	--(II)	
Pyrite		———		
Arsenopyrite		—		
Chalcopyrite		————————-----	---------(II)	
Cubanite		----		
Pyrrhotite		————		
Sphalerite		----		
Tennantite		--		
Molybdenite			--	
Galena			--	
Native gold			--	
Bi-native			--	
Bismuthinite			--	
Tellurobismuthite			--	
Thiosulphate				-----
Malachite				-----
Azurite				----
Fe-hydroxide				---------

1 – after Gaskov et al. (2012); 2 – after Li et al. (2018); minerals in bold were described by the authors

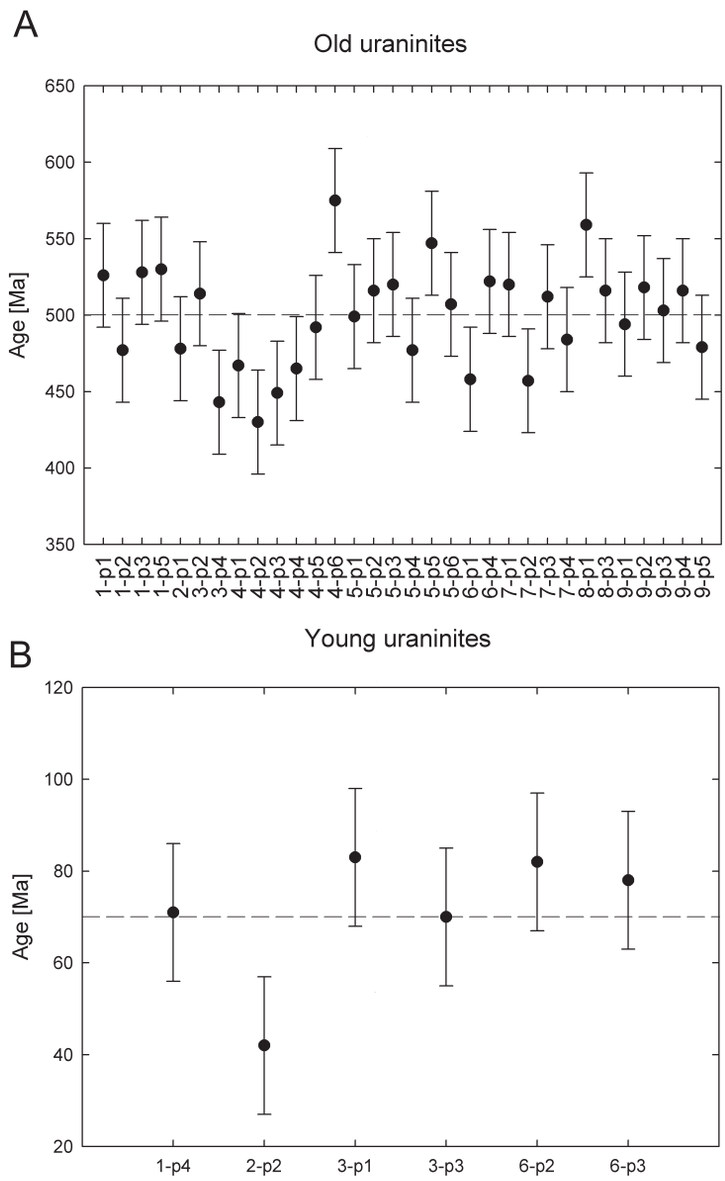

Fig. 9A – ages determined for old uraninites; B – ages determined for young uraninites

level of REE concentration in the Sin Quyen uraninites can be compared to the intrusion related U-deposit (Cuney and Kyser, 2008). High REE concentration is also reported from unconformity-type mineralization (Alexandre et al., 2015). The yttrium content in the analysed uraninite varies from 0.79 to 2.37 wt.% with an average of 1.46 wt.%. The range of Y confirms also an intrusion relationship (Alexandre et al., 2015). The presence of REEs in the uraninite suggests that U and REEs were deposited simultaneously during the ore-forming process.

The average chondrite-normalized curve of REE concentration of older uraninite tends to have weak positive Eu and Lu anomalies (Fig. 10). The REE average spectra of young uraninite show four anomalies including La, Pr, Eu and Lu (Fig. 11). The variations of REE amounts are typical in U deposits as a result of temperature differences (Mercadier et al., 2011). In general, the shape of the average chondrite-normalized curve of REE concentration in old uraninite is similar to spectra of synmetamorphic U deposit (e.g., Kawanga, Botswana; Mistamisk in Canada; Mercadier et al., 2011). This normalized concentration curve is significantly differs in shape from the REE concentration chondrite-normalized curve for allanite, garnet and zircon, presented in the publication by Li et al. (2018). These differences suggested that uraninites were precipitated during the other stage in comparison with the mentioned minerals, which is in good agreement with microscopic observation (e.g., Fig. 6D). A negative Eu anomaly in the chondrite-normalized curve appears only in vein-type and intrusive U deposits (Mercadier et al., 2011). The REE chondrite-normalized curve in uraninite for the IOCG deposit is characterized by a small variation in REE concentration with a small positive Eu anomaly (Fig. 12). It can be explained by different ionic REE radii. The only intermediate REE members have radii of 1.06 Å, which is similar to uranium (1.08 Å). The Eu concentration anomalies can also be explained by the charge compensation, which is

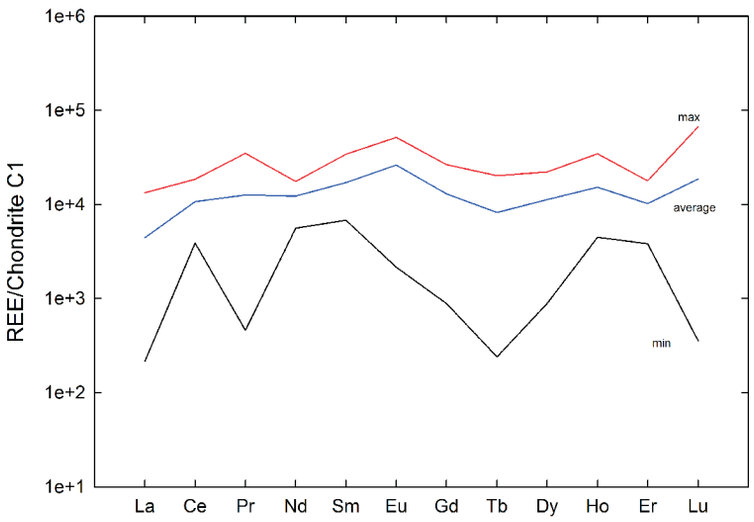

Fig. 10. Chondrite-normalized patterns of REE concentration (max., min. and average for n = 33) in old uraninite

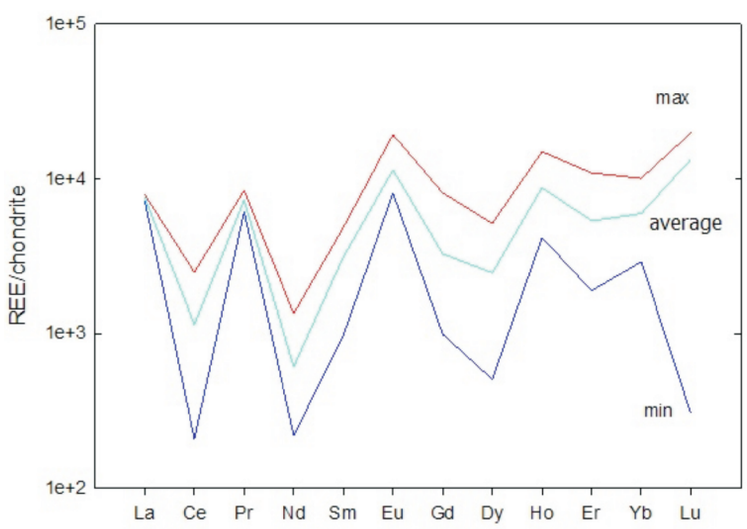

Fig. 11. Chondrite-normalized patterns of REE concentration (max., min. and average for n = 6) in young uraninite

better for two-valence cations (e.g., Eu^{+2}), and by the construction of the outer electron band. Based on it, the shape of the average curve of old uraninite would be very easily explained (Figs. 10 and 11).

TIMING OF ORE MINERALIZATION

As discussed above, electron microprobe analyses and BSE images indicate two compositionally different generations of uraninite at the Sin Quyen deposit. Moreover, the composition of the two generations is relatively constant (Appendix 2). As virtually all Pb in uraninite is produced by the radiogenic decay of U and Th, the consistency in the composition of the two generations of uraninite offers the opportunity to determine the age of uraninite deposition and the formation of the Sin Quyen deposit.

Over the last two decades, techniques have been developed to allow determining an age of U-Th-rich minerals such as uraninite and monazite, including ion microprobe analysis. Chemical dating assumes all Pb in the analysed U-Th-rich mineral formed by radiogenic decay, with no geogenic Pb (Kempe, 2003). Using the electron microprobe data and the original *Jeol* software, absolute age of uraninite was calculated. The Pb-rich uraninite yields ages of 430 to 575 Ma with a mean weighted age of 500 ±33 Ma (n = 33) (Appendix 2, Figs. 8 and 9A). As these uraninite grains are intergrown closely with magnetite and chalcopyrite, it is interpreted as the same stage of IOCG mineralization at Sin Quyen (Table 3).

The Pb-poor uraninite yields an age of 42–83 Ma (n = 6) (Appendix 2, Figs. 8 and 9B), which is interpreted as a recrystallization time; during the period the young hydrothermal event was taking place. Uraninite is commonly recrystallized following initial formation, resulting in a long tail of younger ages

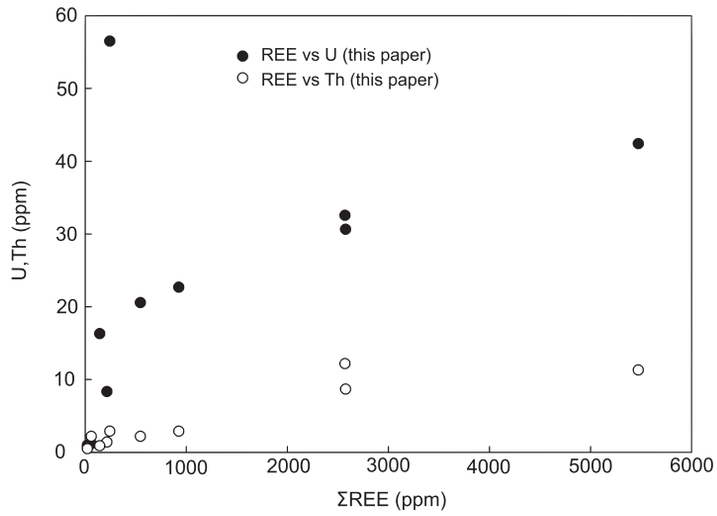

Fig. 12. Chondrite-normalized patterns of REE concentration in old uraninites and allanites, based on WDS quantitative measurements

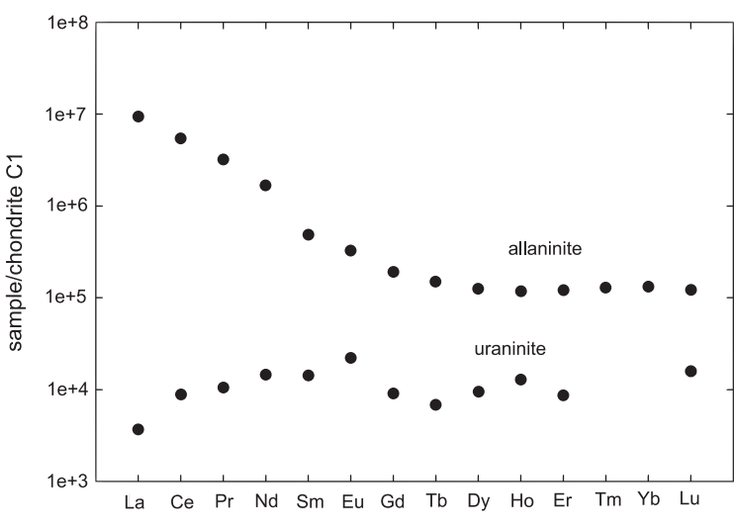

Fig. 13. Relation of U and Th with ΣREE in rock, ore, concentrate and waste samples, based on bulk chemical analyses (ACME)

that have uncertain geological meaning (Mercadier et al., 2011). The age of ~42 Ma, as determined from the low-Pb uraninite, corresponds to the final changes observed in the ore.

Recently (2018), two publications describing the timing of mineralization in the Sin Quyen deposit have appeared (Li et al., 2018; Li and Zhou, 2018b), both using zircon and monazite. These two publications allow better understanding of the whole range of development of ore minerals. The oxygen isotopes described by Li and Zhou (2018b) show different genetic positions of both these minerals, which is in good agreement with crystal parameters of zircon, e.g. elongation l/h close to 1.5. Such zircon crystal elongation is rather typical for metamorphic rocks, which are the host rocks for the Fe-Cu ores. The first stage of mineralization is related to the sodium alteration dated at 841–836 Ma (Li et al., 2018; Li and Zhou, 2018b; Table 3). The $\delta^{18}O$ values of zircon are higher than those presented in magnetite (Li and Zhou, 2018b), which in our opinion exclude simultaneous crystallization of these minerals. Measurement of fluid inclusions shows high temperature above 500°C (Li and Zhou, 2018b), which may suggest participation of metamorphic or magmatic fluids (Taylor, 1974). Alteration of uraninite grains documented by WDS quantitative measurements (Appendix 2, Fig. 8) and BSE images showing well-visible alteration of uraninite grains (Fig. 8) suggests the presence of at least two important stages, which are good documented by the uraninite age dating and fit well to the geological phenomena (Anczkiewicz et al., 2000; Żelaźniewicz et al., 2013).

The determination of absolute age (Appendix 2, Fig. 8) provides new constraints on mineral timing (Table 3), and enables a better understanding of the mineral paragenesis presented by Ta (1975) and McLean (2001). Three stages of magnetite+sulphide formation have been recognized. The first two are the main stages. According to mineralogical studies, most ores were precipitated during the skarn-metasomatic stage, which is the first

stage (Ta, 1975; McLean, 2001). As the Pb- and REE-rich uraninite crystallized together with magnetite and allanite followed by massive chalcopyrite, pyrrhotite, pyrite and cubanite, and is characterized by high concentration of REEs, this uraninite is interpreted to be formed during the early stage of deposition (Table 3). This is also supported by the positive correlation between U-Th and REE (Fig. 13). The hydrothermal stage, as described by Ta (1975) and McLean (2001) as a major sulphide crystallization stage, is interpreted here as a continuation of the first metasomatic stage. Determination of sulphide temperature crystallization is difficult and requires further study. The presence of sphalerite star exsolution in chalcopyrite suggests temperature of sulphide crystallization in the range of 300–500°C (Sugaki et al., 1987; Krismer et al., 2011). This temperature is realistic for the mineral assemblage described in this work. These stages are related to two calk-alkaline granitoids: Po Sen probably of Precambrian age (Bui et al., 2004) and Muong Hum of Paleogene age dated with K-Ar at 30–36 Ma (Hayashi et al., 2009). The Lower Paleozoic age of the Song Chay batholith is also suggested by Żelaźniewicz et al. (2013), which fits very well to the first stage of ore mineralization. The age of 35 Ma (Appendix 2) for the final cooling is proposed by Viola and Anczkiewicz (2009). Żelaźniewicz et al. (2013) also described two types of young granite, both of Paleogene age: calk-alkaline I-type and sub-alkaline A-type. Both types can be responsible for the last stage of ore transformation. Crystallization of uraninites was probably shifted in time in relation to allanite. Based on the shape of an average chondrite-normalized pattern of REE in both allanite and uraninite (Fig. 12), it can be pointed out that uraninite crystals are generally younger (Table 3).

The younger hydrothermal stage overprinted the older one, brought recrystallization of uraninite, and may have introduced elements such as Pb, Au, Ag, Se, Bi and Te. This is confirmed by structures and textures of this assemblage (e.g., Figs. 5 and 7). The youngest stage (Table 3) was developed during weathering responsible for oxidation of some sulphides in the surface environment. The zone of oxidation reached probably 100 metres below the surface, because of vertical position of both rocks and ore.

CONCLUSIONS

Low-grade uranium concentrations have been documented in the deposit. The study of Pieczonka et al. (2015) shows that two different mineral groups are responsible for uranium concentration: allanites and uraninites. In that work, enrichment in U was confirmed by using both field and laboratory measurements. The first group includes two minerals from the allanite group, and probably monazites (Ishihara et al., 2011); however, because of inadequate relatively higher detection limits of both EDS and WDS analyses and low concentration of this element, it is difficult to precisely determine the quantitative content of uranium in these minerals. The presence of uraninite in the association of magnetite-sulphide ores, accompanied by allanite, was documented in the deposit. The differences in REE and uranium concentrations are shown by bulk chemical analyses (Appendix 1) of samples collected from both a waste pond and the deposit. In the case of the Sin Quyen deposit, the relatively high concentration of U and REE in the waste suggests coexistence of all these elements in allanites (Appendix 1A, B) and uraninite (Appendix 2); however, the results from sample W-18 show another possibility. In this sample, the high concentration of uranium (56.51 ppm; Appendix 1A, B) corresponds with low concentration of REE (242.33 ppm; Appendix 2). It can be suggested that mostly uranium oxides are responsible for uranium concentration in the deposit.

In this work, three stages of mineralization have been documented in the deposit that consists of copper ores containing some gold-silver enrichment. In the previous works (Li et al., 2018; Li and Zhou, 2018b), a high-temperature Na-alteration stage 841–836 Ma was documented.

The major stage is skarn-metasomatic (Table 3), which developed in the Late Precambrian and Early Cambrian (575–435 Ma). The younger stage (Table 3) is documented by uraninite II and occurred during Late Cretaceous-Paleocene times (83–42 Ma); however, according to the data of fission-track analyses by Anczkiewicz et al. (2000), the last ductile deformation within the Red River Fault Zone took place ~25 Ma.

The magnetite ore extracted and the magnetite concentrate received are strongly contaminated with high concentration of sulphur, disqualifying it as a market product.

Acknowledgement. The authors are grateful to G. Kozub and A. Włodek from Critical Elements Lab. Faculty of Geology, Geophysics and Environmental Protection UST-AGH Kraków for the WDS analyses, and to T. Ćwiertnia for preparation of graphics. The authors are also grateful to UST-AGH Kraków for financial support, grants Nos. 11.11.140.161 and 11.11.140.645, and University of Mining and Geology (UMG), Hanoi, Vietnam, grant No. 01/2012/HD-HTQTSP.

REFERENCES

Alexandre, P., Kyser, K., Layton-Matthews, D., Joy, B., 2015. Chemical compositions of natural uraninite. The Canadian Mineralogist, **53**: 595–622.

Anczkiewicz, R., Viola, G., Müntener, O., Thirwall, M.F., Villa, I.M., Cuong, N.Q., 2000. Evolution of the Red River Shear Zone deduced from structural and fission track studies of the Day Nui Con Voi massif in North Vietnam. Mineralogical Society of Poland-Special Papers, **17**: 108–110.

Budzyń, B., Yi, K., Lee, S., Kusiak, M.A., Kozub-Budzyń, G., Włodek, A., Konečny, P., Rzepa, G., 2017. Two Madagascar monazite crystals as potential reference materials for U-Pb microanalysis. Mineralogia – Special Papers, **47**: 46.

Bui, P.M., Nguyen, V.H., Phan, V.K., Tran, D.T., 2004. Geology and Mineral Resources of Kim Binh-Lao Cai Sheet, Scale 1:200,000. General Department of Geology and Minerals of Vietnam.

Chen, W.T., Zhou, M.F., Gao, J.F., Hu, R., 2015. Geochemistry of magnetite from Proterozoic Fe-Cu deposits in the Kangdian metallogenic province, SW China. Mineralium Deposita, **50**: 795–809.

Corriveau, L.L., Ootes, H., Mumin, V., Jackson, V., Bennet, J.F., Cremer, J.F., McMartin, I., 2007. Alteration vectoring to IOCG (U) deposits in frontier volcano-plutonic terrain, Canada. In: Proceedings Exploration '07, Fifth Decenniak International Conference on Mineral Exploration: 1171–1177.

Cuney, M., Kyser, T.K., 2008. Recent and not-so-recent developments in uranium deposits and implications for exploration. Mineralogical Association of Canada Short Course Series, **39**.

Dupuis, C., Beaudoin, G., 2011. Discriminant diagrams for iron oxide trace element fingerprinting of mineral deposit types. Mineralium Deposita, **46**: 319–335.

ESCAP, 1990. Report of Economic and Social Commission for Asia and the Pacific, 1990.

Faure, M., Lepvrier, C., Vuong, N.V., Tich, V.V., Lin, W., Chen, Z., 2014. The South China block-Indochina collision: where, when, and how? Journal of Asian Earth Sciences, **79**: 260–274.

Fengli, Y., Yafei, W., Shunfu, L., Xiaofen, L., Pengfei, G., Jiannian, Z., 2014. Comparisons between the Zhuchong Fe-Cu Deposit in Anqing and the IOCG-type Deposits. Acta Geologica Sinica, **88**: 403–404.

Gaskov, I.V., Tran, T.A., Tran, T.H., Pham, T.D., Nevolko, P.A., Pham, N.C., 2012. The Sin Quyen Cu-Fe-Au-REE deposit (northern Vietnam) composition and formation conditions. Russian Geology and Geophysics, **52**: 442–456.

Hayashi, T., Machida, S., Fukusawa, H., Takahashi, K., Nguyen, B.M., Ninh, Q.T., Tran, V.M., Nguyen, D.T., 2009. Age of carbonatite and alkalian magmatism in North Vietnam and its rare earth mineralization. Abstract with Programs 59th Annual Meeting Symposium: Geology and Mineral Resources of Vietnam and Surrounding Region: 21.

Hitzman, M.W., 2000. Iron oxide-Cu Au deposits: what, where, when, and why. In: Hydrothermal Iron Oxide Copper Gold and Related Deposits: a Global Perspective (ed. T.M. Porter): 9–25. PGC Publishing, Adelaide.

Ishihara, S., Hideo, H., Mihoko, H., Pham, N.C., Pham, T.D., Tran, T.A., 2011. Mineralogical and chemical characteristics of the allanite-rich copper and iron ores from the Sin Quyen mine, northern Vietnam. Bulletin of the Geological Survey of Japan, **62**: 197–209.

Janeczek, J., Ewing, R.C., 1995. Mechanisms of lead release from uraninite in the natural fission reactors in Gabon. Geochimica et Cosmochimica Acta, **59**: 1917–1931.

Kempe, U., 2003. Precise electron microprobe age determination in altered uraninite: consequences on the intrusions age and metallogenic significance of the Kirschberg granite (Erzgebirge: Germany). Contribution to Mineralogy and Petrology, **45**: 107–118.

Krismer, M., Vavtar, F., Tropper, P., Sartory, B., Kaindal, R., 2011. Mineralogy, mineral chemistry and petrology of the Ag-bearing Cu-Fe-Pb-Zn sulphide mineralizations of the Pfunderere Berg (South Tyrol, Italy). Australian Journal of Earth Science, **104**: 36–48.

Le, K.P., Nguyen, T.S., Tran, T.N., Lai, M.G., Piestrzynski, A., Pieczonka, J., Jodlowski, P., Nguyen, D.C., Nguyen, V.L., Nguyen, V.N., Do, T.H.T., 2015a. Researching the procedures for survey and assessment of the radioactive environmental impacts due to mining and processing ores at the Sing Quyen cooper mine, Lao Cai province. Materials of the 2-nd International Conference Scientific-Research Cooperation between Vietnam and Poland in Earth Sciences, **4–6**: 359–369.

Le, K.P., Nguyen, T.S., Piestrzyński, A., Pieczonka, J., Jodłowski, P., Nguyen, D.C., Nguyen, V. L., Nguyen, V.N., Do, T.H.T., 2015b. Expansion characteristics of the radioactive materials due to the enrichment and melting the copper alloys at the IOCG Sin Quyen deposit (in Vietnamese). Materials of the National Conference on the occasion of the 70th Anniversary Hanoi: 253–261.

Leloup, P.H., Tapponnier, P., Lacassin, R., 2007. Discussion on the role of the Red River shear zone, Yunan and Vietnam in the continental extrusion of SE Asia. Journal of the Geological Society of London, **164**: 1253–1260.

Li, X.C., Zhou, M.F., 2018a. Hydrothermal alteration of monatzite-(Ce) and chevkinite-(Ce) from the Sin Quyen Fe-Cu-LREE-Au deposit, northwestern Vietnam. American Mineralogist, **102**: 1525–1541.

Li, X.C., Zhou, M.F., 2018b. The nature and origin of hydrothermal REE mineralization in the Sin Quyen deposit, Northwestern Vietnam. Economic Geology, **113**: 645–673.

Li, X.C., Zhou, M.F., Chen, W.T., Zhao, X.F., Tran, M.D., 2018. Uranium-lead dating of hydrothermal zircon and monazite from the Sin Quyen Fe-Cu REE-Au-(U) deposit, northwestern Vietnam. Mineralium Deposita, **53**: 399–416.

McLean, R.N., 2001. The Sin Quyen iron oxide-copper-gold-rare earth oxide mineralization of North Vietnam. In: Hydrothermal iron oxide copper-gold and related deposits: a global perspective 2 (ed. T.M. Porter): 293–301. PGC Publishing, Adelaide.

Mercadier, J., Cuney, M., Lach, P., Boiron, M.C., Bonioure, J., Richard, A., Leisen, M., Kister, P., 2011. Origin of uranium deposits revealed by their rare earth element signature. Terra Nova, **23**: 264–269.

Nguyen, D.C., Le, K.P., Jodłowski, P., Pieczonka, J., Piestrzyński, A., Duong, V.H., Nowak, J., 2016. Natural Radioactivity at the Sin Quyen iron oxide copper gold deposit in North Vietnam. Acta Geophysica, **64**: 2305–2321.

Pearson, F.J., Rightmire, C.T., 1980. Sulphur and oxygen isotopes in aqueous sulphur compounds. In: The Terrestrial Environment (eds. P. Fritz and J.Ch. Fontes): 227–258. Elsevier, Amsterdam.

Pham, N.C., Ishiyama, D., Tran, T.A., Sera, K., 2011. Mineralogical and geochemical characteristics of rare metals bearing Na Bop, Lung Hoai, Nason and Sin Quyen Base metal deposits, Northern Vietnam. NMCC Annual Report, **18**: 49–55.

Phan, T.H., 2015. The Ngoi Chi Formation in the Phan Si Pan area of northwest Vietnam revealed by zircon U-Pb age and Hf isotope composition. Acta Geoscientica Sinica, **36**: 755–760.

Pieczonka, J., Piestrzyński, A., Le, K.P., Nguyen, D.C., Jodłowski, P., 2015. Rare Earth, radioactive and selected elements in the iron oxide copper gold Sin Quyen deposit in North Vietnam. In: Viet-Pol 2015 second international conference on scientific research cooperation between Vietnam and Poland in Earth Sciences: 331–353.

Pieczonka, J., Piestrzyński, A., Nguyen, D.C., Le, K.P., Hao, D.V., 2017. IOCG Sin-Quyen deposit, Lao Cai, N-Vietnam. Mineral resources to discover. Proceedings, 14th Biennial SGA Meeting, Quebec, Canada: 955–959.

Pyle, J.M., Spear, F.S., Wark, D.A., 2002. Electron microprobe analysis of REE in apatite, monazite and xenotime: protocols and pitfalls. Reviews in Mineralogy and Geochemistry, **48**: 337–362.

Sugaki, A., Kitakaze, A., Kojima, S., 1987. Bulk composition of intimate intergrowth of chalcopyrite and sphalerite and their genetic implications. Mineralium Deposita, **22:** 26–32.

Ta, V.D., 1975. Report of geological surveys and their results performed at the IOCG Sin Quyen deposit in Lao Cai, North Vietnam. Main Department of Geology of Vietnam (in Vietnamese): 318.

Tapponnier, P., Lacassin, R., Leloup, H., Scharer, U., Zhong, D., Liu, X., Ji, S., Zhang, L., Zhong, J., 1990. The Ailaoshan-Red river metamorphic belt: Tertiary left-lateral shear between Indochina and South China. Nature, **343**: 431–437.

Taylor, H.P., 1974. The application of oxygen and hydrogen isotopes studies to problem of hydrothermal alteration and ore deposition. Economic Geology, **69**: 843–883.

Thode, H.G., 1991. Sulphur isotopes in nature and the environment: an overview. In: Stable Isotopes in the Assessment of Natural and Anthropogenic Sulphur in the Environment (ed. H.R. Krouse and V.A. Grinenko): 1–26. John Wiley and Sons Lid.

Tran, T.H., 2007. Inplate magmatism in Northern Vietnam and its metallogeny. Sc.D. thesis, IGM SO RAN, Novosibirsk.

Viola, G., Anczkiewicz, R., 2009. Exhumation history of the Red River shear zone in northern Vietnam: new insights zircon and apatite fission-track analysis (in Vietnamese). In: Dianamic Geolog, Kainozoi N-Vietnam (eds. T.Y. Nguyen, A. Tokarski, T.H. Tran, A. Zuchiewicz, T.A. Tran, A. Świerczewska and Q.C. Nguyen): 150–164.

Zhao, X.F., Zhou, M.F., 2011. Fe-Cu deposits in the Kangdian region, SW China: a Proterozoic IOCG (iron-oxide-copper-gold) metallogenic province. Mineralium Deposita, **46**: 731–747.

Żelaźniewicz, A., Tran, T.H., Larionov, A.N., 2013. The significance of geological and zircon age data derived from the wall rocks of the Ailao Shan-Red River Shear Zone, NW Vietnam. Journal of Geodynamics, **69**: 122–139.